Texas A&M University
Mechanical Engineering Department
Turbomachinery Laboratory

A METHOD FOR IDENTIFICATION OF FORCE COEFFICIENTS IN FLEXIBLE ROTOR-BEARING SYSTEMS

Research progress Report to the Turbomachinery Research Consortium

by

Luis San Andrés
Professor

TRC-B&C-2-03

May 2003

TRC Project:
Identification of Bearing Support Force Coefficients from Rotor responses due to Imbalances and Impact Loads

A METHOD FOR IDENTIFICATION OF FORCE COEFFICIENTS IN FLEXIBLE ROTOR-BEARING SYSTEMS

Executive Summary

Field identification of bearing support parameters is important for adequate interpretation of rotating machinery performance and necessary to calibrate predictions from restrictive physical models. Field identification is also promising for condition monitoring and troubleshooting, and in the near future for self-adapting rotor-bearing systems.

A simple method for estimation of (bearing) support force coefficients in flexible rotor-bearing systems is detailed. The method requires of two independent tests with known mass imbalance distributions and the measurement of the rotor motion (amplitude and phase) at locations close to the supports. The procedure relies on the modeling of the rotor structure and finds the bearing transmitted forces as a function of observable quantities. Solving a simple set of algebraic equations identifies synchronous stiffness and damping force coefficients. Numerical simulations demonstrate perfect parameter identification for a model rotor-bearing system.

Imbalance response measurements conducted with a two-disk flexible rotor supported on two-lobe fluid film bearings allow validation of the identification method estimations. Predicted (linearized) bearing force coefficients agree reasonably well with the parameters derived from the test data. Note that the rotor motions at the support locations are of large magnitude, close to the fluid film bearing radial clearance. Thus, the estimated test coefficients do not correspond with conventional linearized force coefficients.

The method advanced does not add mathematical complexity nor requires of additional instrumentation than that already available in most high performance turbomachinery.

Acknowledgements

The Principal Investigator thanks Mr. Chris Holt (Active Power) for sharing his MATHCAD Finite Element rotordynamics code. The significant contribution of Dr. Oscar de Santiago (Dresser Rand), who conducted the imbalance response measurements and advanced the earlier versions of the identification procedures, is also acknowledged. The recognition and support of STLE (Society of Tribologists and Lubrication Engineers) are welcome. STLE provided a graduate fellowship to Mr. Kishore Balantrapu, Research Assistant.

Table of Contents

List of Tables

List of Figures

Nomenclature

D, L_b, c_b, r_p	Two lobe bearing length, diameter, clearance and preload [m].
$C_{\alpha\beta}, K_{\alpha\beta},$	Bearing support damping and stiffness coefficients [N/m, Ns/m] αβ=x,y
$F_x, F_y, M_{\beta x}, M_{\beta y}$	Lateral forces [N] and moments [Nm] at rotor stations
(m, u, ϕ)	Imbalance mass [kg], radius [m], and phase angle [rads]
$(x,y), (\beta_x, \beta_y)$.	Rotor displacements [m] and rotations [rads] at each station
N_e, N_s	Number of elements and stations in rotor
t	Time [s]
μ	Lubricant viscosity [Pa-s]
Ω	Rotor speed [rad/s]
ω	Excitation frequency [rad/s]

Vectors/matrices

$\mathbf{f_B}$	Rotor forces [N] at support locations
$\mathbf{H_B}$	Bearing support impedance matrix [N/m]
$\mathbf{H_R}$	Rotor impedance (dynamic stiffness) matrix [N/m]
$\mathbf{H_{Rab}}$ a,b=1,2,3	Partitions of rotor impedance matrix $\mathbf{H_R}$ [N/m]
$\mathbf{M_e, K_e, G_e}$	Rotor element mass, stiffness and gyroscopic matrices
$\mathbf{M, K_R, G}$	Global (rotor) mass, stiffness and gyroscopic matrices
Q, q	Vectors of generalized forces and rotor displacements.
$\mathbf{z_B}$	*(x,y)* complex rotor displacements at supports
$\mathbf{z_u}$	Complex rotor displacements

Subindices

B_1, B_2	Bearings supports, 1 and 2

Introduction

Experimental identification of fluid film bearing parameters is critical for adequate interpretation of rotating machinery performance and necessary to validate or calibrate predictions from restrictive computational fluid film bearing models. Parameter identification in the field is also promising for condition monitoring and troubleshooting, and in the near future for self-adapting rotor-bearing control systems.

De Santiago and San Andrés [1] describe a method suitable for field implementation that allows identification of synchronous bearing support parameters (force coefficients) from recorded rotor responses to known imbalances. The experimental validation is conducted on a test rotor supported on two dissimilar bearing supports, both mechanically complex, each comprising a hydrodynamic film bearing in series with a squeeze film damper and elastic support structure. The identification procedure requires a minimum of two different imbalance distributions for identification of force coefficients from the two bearing supports. The recorded rotor responses show minimal cross-coupling effects, as also predicted by analysis, and the identification procedure disregards cross-coupled force coefficients thereby reducing its sensitivity to small variations in the measured response. The procedure renders reasonably accurate force coefficients in the speed range between 1,500 and 3,500 rpm, enclosing the rotor-bearing system first critical speed. The identified direct force coefficients are in accordance with those derived from the impact load excitations presented in a companion paper [2].

De Santiago and San Andrés [2] also introduce a simple procedure, with potential as a field resource, for identification of bearing support parameter from recorded transient rotor responses due to impact loads. The method is applied to a test rotor supported on a pair of mechanically complex bearing supports, each comprising a tilting pad bearing in series with an integral squeeze film damper. Identification of frequency dependent bearing force coefficients is good at a rotor speed of 2,000 rpm. Stiffness coefficients are best identified in the low frequency range (below 25 Hz) while damping coefficients are best determined in the vicinity of the first natural frequency (48 Hz) of the rotor bearing system. The procedure shows that using multiple-impact frequency averaged rotor responses reduces the variability in the identified parameters. The identification of frequency-dependent force coefficients at a constant rotor speed is useful to assess rotor-bearing system stability. Note that the procedures introduced in [1] and [2] are restricted to a rigid rotor configuration.

De Santiago [3] reviews the literature relevant to bearing and rotor support force parameters. In most cases, methods are restricted to the laboratory environment and strictly applicable to rigid rotor configurations and identical bearing supports. Time and frequency domain based parameter identification procedures are based on the seminal works of Goodwin[4] and Nordmann [5] and consider the bearing or support as a two degree of freedom system (x,y) with readily available (measured) support transmitted forces and rotor displacements from which impedances (or mobilities) are obtained. Curve fits to the appropriate transfer functions evidence the support parameters, stiffness and damping.

Actual rotating machinery often features bearing supports that are different on each end of a rotor. Furthermore, nearly all rotors are flexible and not symmetrical, and the bearings on both ends carry different static loads. In overhung rotors, the load differences can be dramatic. Thus, bearing force coefficients differ largely between the drive and free ends of a rotor (even in the case of identical bearings). Thus, it is necessary to extend the previous methods by including the effect of rotor dynamics if in-situ identification is to become viable (without means to measure transmitted forces through the bearings).

Ctiwari and Vyas [6] and Maslen et al. [7, 8] introduce complicated non-linear iterative procedures to extract parameters in flexible rotor - bearing systems. These procedures relying on rotor displacement measurements acknowledge the difficulties on accurate and reliable measurements of transmitted loads at the bearings, for example, in actual rotating machinery systems. This limitation may change in the near future with the application of relatively inexpensive non-intrusive micro strain gauge & fiber optic smart sensors for measurement of transmitted loads.

Lees et al [9] and Feng and Hahn [10, 11], on the other hand, forward simple direct methods to identify rotor support (bearing and pedestal) force coefficients from running machine data, i.e. response to synchronous imbalances. The procedures rely on a reasonably good model of the rotor (elastic and mass properties) and accurate measurements of the rotor response (amplitude and phase) at the locations of interest. Parameter identification follows from estimations of the rotor forces at the supports, and in conjunction with recorded synchronous filtered rotor responses. In general, the system of equations generated by imbalance excitations tends to be ill conditioned; and most experimental identifications show considerable scatter of estimated parameters [3, 4]. In spite of the known limitations, this method continues to appeal as an in-situ identification procedure since it does not require external load excitation and is ready for implementation in instrumented rotor bearing systems (vibration sensor conditioned).

The key features of a successful method for ready field implementation are minimal external equipment, little or no changes to existing hardware, and the use of measuring instruments commonly used in machine protection and monitoring. The present development extends the model introduced by de Santiago [3] to flexible rotor bearing systems and advances a simple methodology to identify bearing or support (pedestal) parameters from imbalance response measurements. A good rotor model (elastic and mass properties) is mandatory to represent correctly the (non observable or not measured) degrees of freedom. Two (known) linearly independent rotor imbalance distributions and the measurement of the rotor motion near the bearing supports provides sufficient information to accurately estimate synchronous bearing force coefficients (stiffness and damping).

Equations of motion for flexible rotor – bearing supports

Figure 1 depicts the configuration of a flexible rotor supported on two bearings. The rotor is partitioned into a number (N_e) of finite elements. Rotor motion coordinates at the ends of each element (stations) are defined by lateral displacements (*x,y)* and rotations (β_x, β_y). Indices B_1 and B_2 denote the stations location of the bearing supports.

In its most general form the equations of motion for a rotor-bearing system are [12]:

$$\mathbf{M}\ddot{\mathbf{q}} + \mathbf{C}\dot{\mathbf{q}} - \Omega\mathbf{G}\dot{\mathbf{q}} + \mathbf{K}\mathbf{q} = \mathbf{Q}(t) \tag{1}$$

where **M, C, G,** and **K** are the global matrices of inertia, damping, gyroscopics and stiffness coefficients, respectively. **Q** and **q** denote the vectors of generalized forces and displacements and Ω represents the rotor speed.

Timoshenko beam finite element matrices [13, 14] are defined in terms of the rotor elasto-massic properties. Appendix A details these matrices for each rotor finite element. The global rotor mass, **M,** stiffness, $\mathbf{K_R}$, damping, $\mathbf{C_R}$, and gyroscopic moments, **G,** matrices are assembled as

$$\mathbf{M} = \bigcup_{e=1}^{N_e} \mathbf{M}_e, \mathbf{K}_\mathbf{R} = \bigcup_{e=1}^{N_e} \mathbf{K}_e, \mathbf{G} = \bigcup_{e=1}^{N_e} \mathbf{G}_e, \mathbf{C}_\mathbf{R} = \bigcup_{e=1}^{N_e} \mathbf{C}_e \tag{2}$$

The vectors of rotor displacements and generalized external forces are

$$\begin{aligned} \mathbf{q} &= \left[\mathbf{q_1} \;..\; \mathbf{q}_{\mathbf{B}_1} \;..\; \mathbf{q}_{\mathbf{B}2} \;..\; \mathbf{q}_{\mathbf{N}_s}\right]^{\mathrm{T}};\quad \mathbf{q}_i = \left[x_i \quad y_i \quad \beta_x \quad \beta_y\right]^T, i = 1..N_s \\ \mathbf{Q} &= \left[\mathbf{Q_1} \;..\; \mathbf{Q}_{\mathbf{B}_1} \;..\; \mathbf{Q}_{\mathbf{B}2} \;..\; \mathbf{Q}_{\mathbf{N}_s}\right]^{\mathrm{T}};\quad \mathbf{Q}_i = \left[F_{x_i} \quad F_{y_i} \quad M_{\beta_x} \quad M_{\beta_y}\right]^T, i = 1..N_s \end{aligned} \tag{3}$$

The damping **C** and stiffness **K** matrices combine the effects of the rotor and the bearing supports, i.e.

$$\mathbf{K} = \mathbf{K_R} + \begin{bmatrix} \mathbf{0} & .. & .. & .. & .. \\ .. & \mathbf{K}_{\mathbf{B}_1} & .. & .. & .. \\ \mathbf{0}.. & .. & .\mathbf{0} & .. & .. \\ .. & .. & .. & \mathbf{K}_{\mathbf{B}_2} & .. \\ .. & .. & .. & .. & \mathbf{0} \end{bmatrix}; \mathbf{C} = \mathbf{C_R} + \begin{bmatrix} \mathbf{0} & .. & .. & .. & .. \\ .. & \mathbf{C}_{\mathbf{B}_1} & .. & .. & .. \\ \mathbf{0}.. & .. & .\mathbf{0} & .. & .. \\ .. & .. & .. & \mathbf{C}_{\mathbf{B}_2} & .. \\ .. & .. & .. & .. & \mathbf{0} \end{bmatrix} \tag{4}$$

The support stiffness $\mathbf{K_B}$ and damping $\mathbf{C_B}$ matrices contain the following (yet undetermined) coefficients:

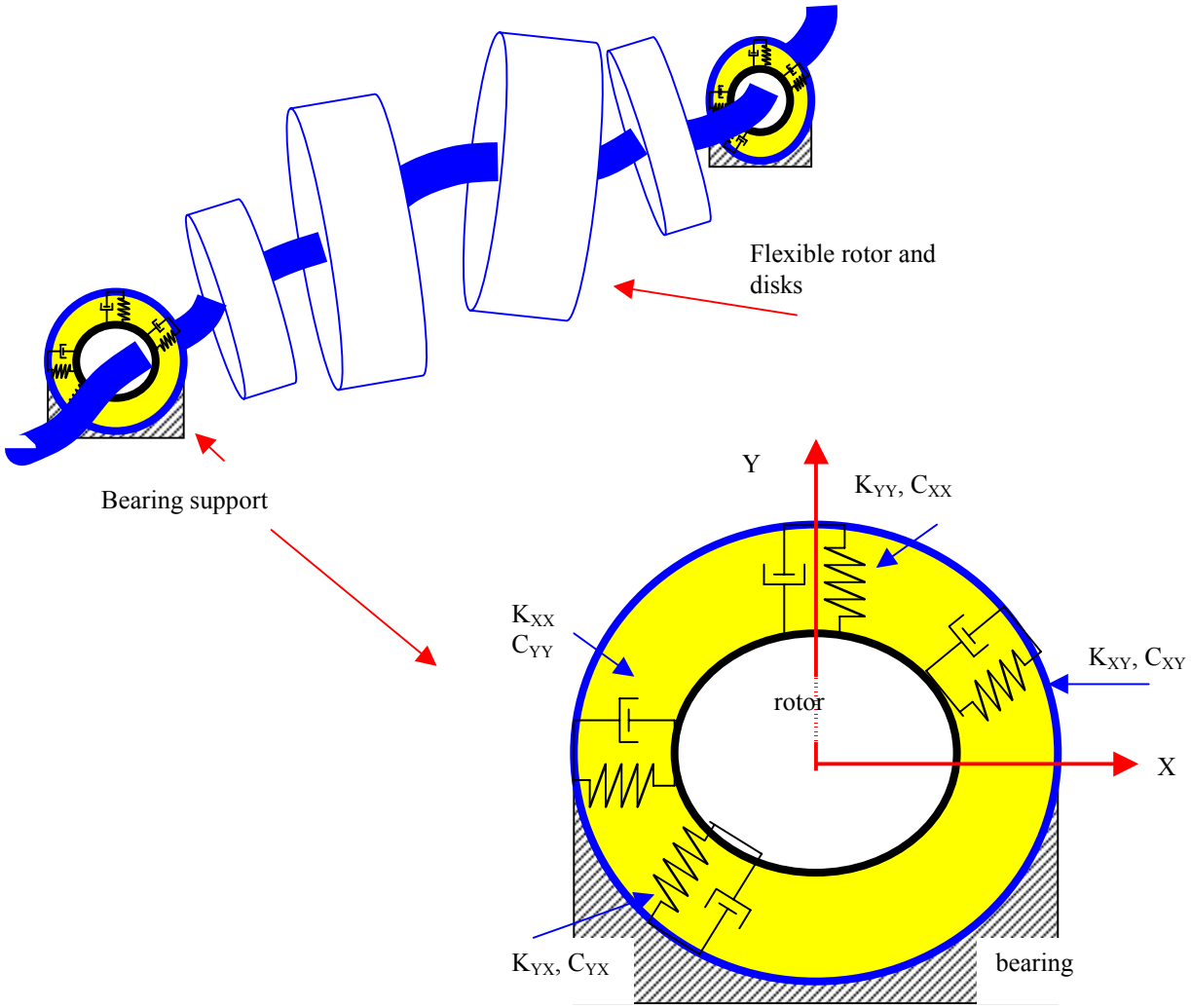

Figure 1 Schematic view of elastic rotor on flexible-damped (bearing) supports and idealization of support force coefficients

$$\mathbf{K_{Bi}} = \begin{bmatrix} K_{xx} & K_{xy} \\ K_{yx} & K_{yy} \end{bmatrix}_i \; ; \; \mathbf{C_{Bi}} = \begin{bmatrix} C_{xx} & C_{xy} \\ C_{yx} & C_{yy} \end{bmatrix}_i \quad i=1,2 \tag{5}$$

The (bearing) support force coefficients are functions of the operating conditions (rotor speed, static load magnitude and orientation), geometry (length, diameter, clearance), and lubricant feed conditions and material properties in a thin film bearing.

Consider periodic forced excitations with frequency (ω). Rotor imbalance is typical with the frequency of excitation coinciding with rotor speed, i.e. $\omega=\Omega$. At rotor station (s), an imbalance mass (m) at radius ($\underline{u}$) generates lateral forces equal to

$$\begin{Bmatrix} F_x \\ F_y \end{Bmatrix}_s = m u \omega^2 \begin{Bmatrix} \cos(\omega t+\phi) \\ \sin(\omega t+\phi) \end{Bmatrix} = m u \omega^2 \, e^{i\omega t} \, e^{i\phi} \begin{Bmatrix} 1 \\ -i \end{Bmatrix} \tag{6}$$

In general, $\mathbf{Q}(t)=\mathbf{Q}_u \, e^{i\omega t}$, and the rotor response has the same frequency as the excitation, i.e. $\mathbf{q}(t)=\mathbf{q}_u \, e^{i\omega t}$. Then, the equations of motion (1) reduce to the algebraic form:

$$\left[\mathbf{K}-\omega^2\mathbf{M}+\mathrm{i}\,\omega\mathbf{C}-\mathrm{i}\;\omega\;\Omega\;\mathbf{G}\right]\mathbf{q}_u=\mathbf{Q}_\mathrm{u} \tag{7}$$

Procedure for identification of support force coefficients

The method to identify the support parameters, stiffness and damping, is based on the measurement of the rotor displacements due to known imbalances at locations near to the supports. The imbalance distribution $(m, u, \phi)_{a=1..k}$ determines the displacements at the bearings supports

$$\mathbf{z}_{\mathbf{B}_1}=\begin{bmatrix} x_{B_1} \\ y_{B_1} \end{bmatrix}=\begin{bmatrix} x_{C_1}-i\,x_{S_1} \\ y_{B_1}-i\,y_{S_1} \end{bmatrix};\; \mathbf{z}_{\mathbf{B}_2}=\begin{bmatrix} x_{B_2} \\ y_{B_2} \end{bmatrix}=\begin{bmatrix} x_{C_2}-i\,x_{S_2} \\ y_{B_2}-i\,y_{S_2} \end{bmatrix} \tag{8}$$

where $\{x_c, x_s\}$ are the displacements related to the harmonic functions cos(ωt) and sin(ωt), respectively.

The algebraic system of equations (7) is reordered to bring the recorded support motions ($\mathbf{z}_{\mathbf{B}_1}, \mathbf{z}_{\mathbf{B}_2}$) into the upper rows, 1 through 4. Matrix permutation operations, i.e. exchange of rows and columns, lead to the following set of equations

$$\mathbf{H}_{\mathbf{R}\ (\omega,\,\Omega)}\begin{Bmatrix} \mathbf{z}_{\mathbf{B}_1} \\ \mathbf{z}_{\mathbf{B}_2} \\ \mathbf{z}_\mathbf{u} \end{Bmatrix}+\begin{bmatrix} \mathbf{H}_{\mathbf{B}_1} & \mathbf{0} & \mathbf{0} \\ \mathbf{0} & \mathbf{H}_{\mathbf{B}_2} & \mathbf{0} \\ \mathbf{0} & \mathbf{0} & \mathbf{0} \end{bmatrix}\begin{Bmatrix} \mathbf{z}_{\mathbf{B}_1} \\ \mathbf{z}_{\mathbf{B}_2} \\ \mathbf{z}_\mathbf{u} \end{Bmatrix}=\begin{Bmatrix} \mathbf{0} \\ \mathbf{0} \\ \overline{\mathbf{Q}}_\mathbf{u} \end{Bmatrix} \tag{9}$$

where

$$\mathbf{H}_{\mathbf{R}\ (\omega,\Omega)}=\left[\overline{\mathbf{K}}_\mathbf{R}-\omega^2\,\overline{\mathbf{M}}_\mathbf{R}+i\;\omega\,\overline{\mathbf{C}}_\mathbf{R}-i\;\omega\;\Omega\;\overline{\mathbf{G}}\right] \tag{10}$$

is the dynamic rotor stiffness matrix (over bars denote the reordered matrix), and

$$\mathbf{H}_{\mathbf{B}_1}=\mathbf{K}_{\mathbf{B}_1}+i\,\omega\mathbf{C}_{\mathbf{B}_1};\;\mathbf{H}_{\mathbf{B}_2}=\mathbf{K}_{\mathbf{B}_2}+i\,\omega\mathbf{C}_{\mathbf{B}_2} \tag{11}$$

represent the supports impedance matrices. The generalized load vector $\mathbf{Q_u}$ is known from the imbalance distribution, while the vector $\mathbf{z_u}$ represents the vector of unknown rotor displacements. These rotor displacements are not observable or measured, i.e. at the stations not coinciding with the bearing supports.

The rotor impedance (dynamic stiffness) matrix $\mathbf{H_R}$, depending on both excitation frequency (ω) and rotor speed (Ω), is partitioned into the following six submatrices

$$\mathbf{H_R} = \begin{bmatrix} \mathbf{H_{R11}} & \mathbf{H_{R12}} & \mathbf{H_{R13}} \\ \mathbf{H_{R21}} & \mathbf{H_{R22}} & \mathbf{H_{R23}} \\ \mathbf{H_{R31}} & \mathbf{H_{R32}} & \mathbf{H_{R33}} \end{bmatrix} \tag{12}$$

For example, $\mathbf{H_{R21}} \neq \mathbf{H_{R12}^T}$, due to the gyroscopic and viscous damping effects in the rotor. Substitution of (12) into equation (9) gives

$$\begin{bmatrix} \mathbf{H_{R11}} & \mathbf{H_{R12}} & \mathbf{H_{R13}} \\ \mathbf{H_{R21}} & \mathbf{H_{R22}} & \mathbf{H_{R23}} \\ \mathbf{H_{R31}} & \mathbf{H_{R32}} & \mathbf{H_{R33}} \end{bmatrix} \begin{Bmatrix} \mathbf{z_{B_1}} \\ \mathbf{z_{B_2}} \\ \mathbf{z_u} \end{Bmatrix} = \begin{Bmatrix} -\mathbf{H_{B_1}}\,\mathbf{z_{B_1}} \\ -\mathbf{H_{B_2}}\,\mathbf{z_{B_2}} \\ \overline{\mathbf{Q}}_\mathbf{u} \end{Bmatrix} \tag{13}$$

The support motions ($\mathbf{z_{B_1}}, \mathbf{z_{B_2}}$) and the load vector $\{\overline{\mathbf{Q}}_\mathbf{u}\}$ are known. Thus, from the third of equations [13], the (internal) rotor displacements $\mathbf{z_u}$ are:

$$\mathbf{z_u} = \mathbf{H_{R33}^{-1}} \{\overline{\mathbf{Q}}_\mathbf{u} - \mathbf{H_{R31}}\,\mathbf{z_{B_1}} - \mathbf{H_{R32}}\,\mathbf{z_{B_2}}\} \tag{14}$$

Now, define the following generalized rotor forces at the bearing locations

$$\begin{aligned} -\mathbf{f_{B_1}} &= \mathbf{H_{R11}}\,\mathbf{z_{B_1}} + \mathbf{H_{R12}}\,\mathbf{z_{B_2}} + \mathbf{H_{R13}}\,\mathbf{z_u} \\ -\mathbf{f_{B_2}} &= \mathbf{H_{R21}}\,\mathbf{z_{B_1}} + \mathbf{H_{R22}}\,\mathbf{z_{B_2}} + \mathbf{H_{R23}}\,\mathbf{z_u} \end{aligned} \tag{15}$$

and write the first two equations in (13) as

$$\mathbf{H_{B_1}}\ \mathbf{z_{B_1}} = \mathbf{f_{B_1}}\ ; \quad \mathbf{H_{B_2}}\ \mathbf{z_{B_2}} = \mathbf{f_{B_2}} \tag{16}$$

Each of these equations represent two algebraic equations (*x,y)*. However, the number of (complex) bearing parameters is four at each support location. Two (known) mass imbalances at selected rotor positions will produce two rotor responses. These imbalances must be linearly independent, as defined in (2). The imbalance distributions $[(m,u,\phi)_k]_{j=1,2}$ produce the support displacements $\{\mathbf{z_{B_{11}}}, \mathbf{z_{B_{21}}}\}$, *and* $\{\mathbf{z_{B_{12}}}, \mathbf{z_{B_{22}}}\}$, and corresponding reaction forces $\{\mathbf{f_{B_{11}}}, \mathbf{f_{B_{21}}}\}$, and $\{\mathbf{f_{B_{12}}}, \mathbf{f_{B_{22}}}\}$.

Hence, the equations for each support impedance become

$$\mathbf{H}_{\mathbf{B}_1}\left[\mathbf{z}_{\mathbf{B}_{11}} \quad \mathbf{z}_{\mathbf{B}_{12}}\right]=\left[\mathbf{f}_{\mathbf{B}_{11}} \quad \mathbf{f}_{\mathbf{B}_{12}}\right] ; \mathbf{H}_{\mathbf{B}_2}\left[\mathbf{z}_{\mathbf{B}_{21}} \quad \mathbf{z}_{\mathbf{B}_{22}}\right]=\left[\mathbf{f}_{\mathbf{B}_{21}} \quad \mathbf{f}_{\mathbf{B}_{22}}\right] \tag{17}$$

, and the support impedance coefficients are determined by solving

$$\mathbf{H}_{\mathbf{B}_1}=\begin{bmatrix} K_{xx}+i\omega C_{xx} & K_{xy}+i\omega C_{xy} \\ K_{yx}+i\omega C_{yx} & K_{yy}+i\omega C_{yy} \end{bmatrix}_{B_1}=\left[\mathbf{f}_{\mathbf{B}_{11}} \quad \mathbf{f}_{\mathbf{B}_{12}}\right]\left[\mathbf{z}_{\mathbf{B}_{11}} \quad \mathbf{z}_{\mathbf{B}_{12}}\right]^{-1} \tag{18}$$

for bearing support 1. A similar equation arises for bearing 2.

A further simplification follows in the case when both bearing supports provide identical force coefficients, i.e. $\mathbf{H_{B1}=H_{B2}}$. This case results when both bearings have the same geometry, including film clearance, lubricant properties, and support the same static load. Adding equations (17) leads to the following identification equation

$$\mathbf{H}_{\mathbf{B}_1}=\mathbf{H}_{\mathbf{B}_2}=\left[\mathbf{f}_{\mathbf{B}_{11}}+\mathbf{f}_{\mathbf{B}_{21}} \quad \mathbf{f}_{\mathbf{B}_{12}}+\mathbf{f}_{\mathbf{B}_{22}}\right]\left[\mathbf{z}_{\mathbf{B}_{11}}+\mathbf{z}_{\mathbf{B}_{21}} \quad \mathbf{z}_{\mathbf{B}_{12}}+\mathbf{z}_{\mathbf{B}_{22}}\right]^{-1} \tag{19}$$

Note that the reliable support parameter identification depends on the accuracy of the rotor mass imbalance distribution and the measurement of the rotor response at locations near to the bearing supports. De Santiago [3] details the do's and don'ts for appropriate identification, including a discussion of on the signal amplitude/noise ratio, the matrix conditioning assuring proper inverse calculations, etc.

A computer program in MATHCAD® was created to model the rotor and bearing supports, to calculate free-free and pin-pin mode rotor natural frequencies, and to predict the imbalance response for varying rotor speeds. A second program collects the rotor model information and the (predicted or measured) imbalance responses at the bearing supports and proceeds to identify the support coefficients over a range of rotor speeds. The MATHCAD software imbalance response predictions are verified against XLTRC[2] model and response predictions.

A description of the test rig used for measurement of imbalance response from a flexible rotor supported on two identical cylindrical fluid film bearings follows. De Santiago [3] conducted the measurements and reported bearing force coefficients using a simpler lumped parameter flexible rotor model. The following section is reproduced with permission from [3].

Description of test rig

The test rig used for identification of bearing force coefficients from imbalance response measurements comprises a two-disk steel rotor supported on a pair of two-lobe journal bearings, as shown in Figure 2. Aluminum housings accommodate the test bearings and are bolted to a 50.4 mm (2 in) thick aluminum table. A 0.74 kW (1 HP), DC motor provides power to the shaft through a multiplier belt and pulley mechanism, and is able to drive the rotor up to 8,000 rpm. An electronic controller built-in to the rig allows for speed and torque control. A hinged plate covering the test rotor and bearing housings provides safety during the rig operation. The rig is bolted to a steel plate laying on padding material for isolation from the laboratory floor.

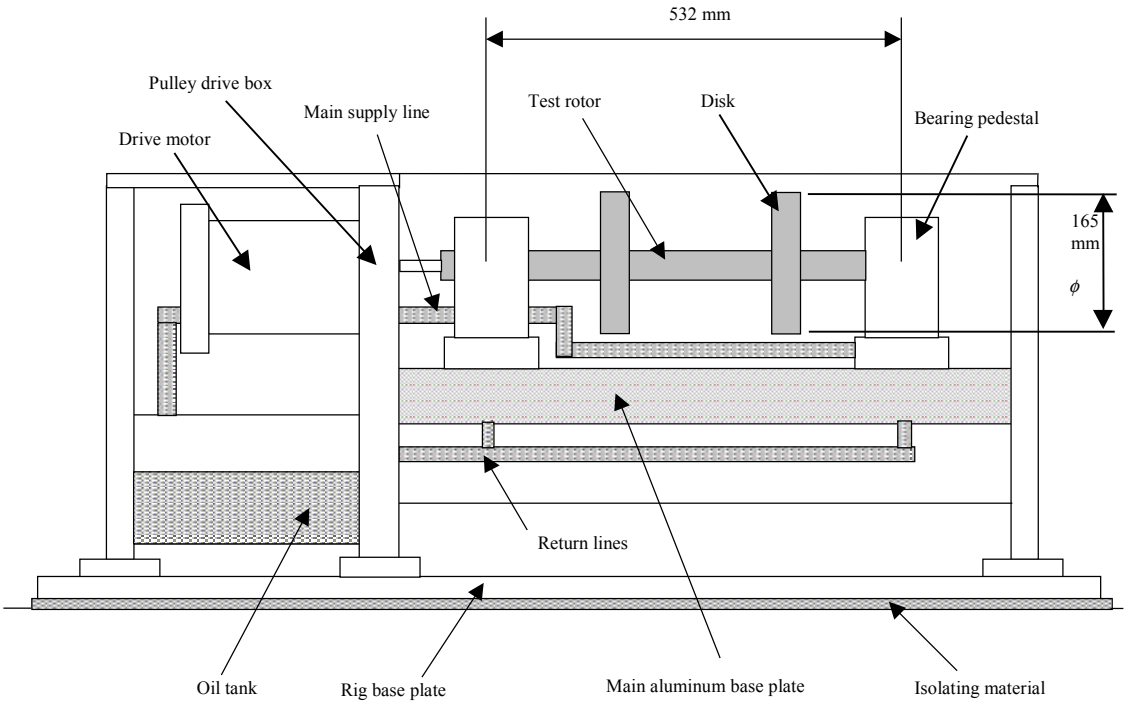

Figure 2 Test rig for imbalance response of flexible rotor supported on fluid film bearings

The test rotor consists of a shaft, 25.4 mm (1.0 in) of main diameter and 640 mm (25.2 in) long, with a bearing span of 532 mm (20.95 in). Figure 3 details the rotor geometry and Table 1 summarizes the rotor main dimensions and measured inertia properties. The shaft has three annular inserts mounted along the shaft within the bearing span. Massive disks can be fitted onto the annular inserts rendering different rotor configurations. For the experiments herein presented, the rotor features two disks attached to the shaft, 280 mm (11.0 in) apart from each other and centered in the bearing span. The shaft has rectified surfaces at the bearing locations and a notched groove at one end where a flexible coupling drives the shaft.

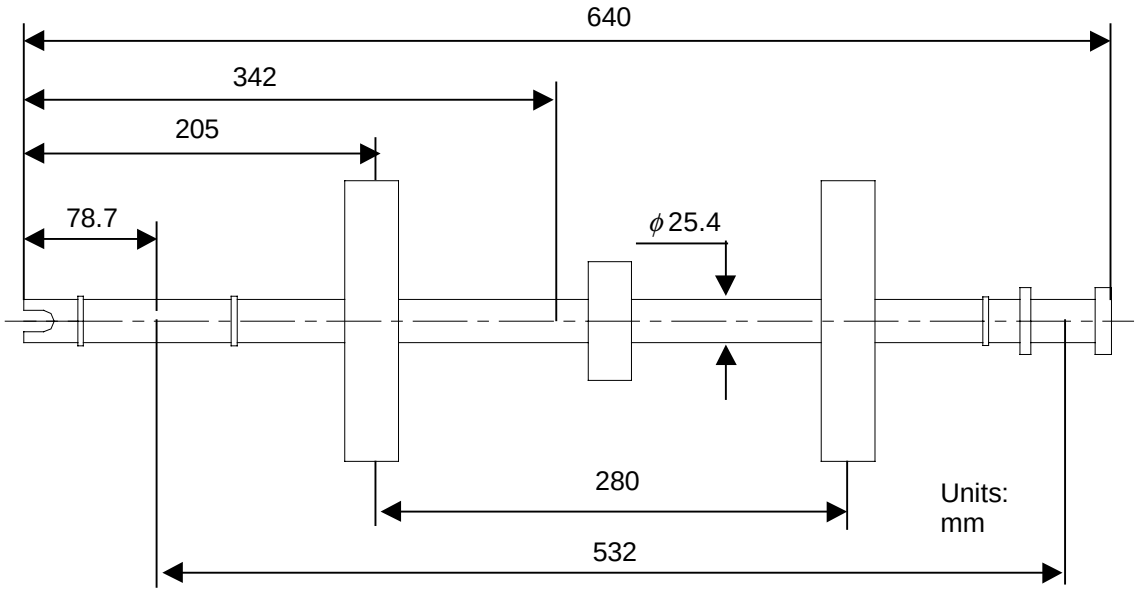

Figure 3 Flexible rotor for bearing parameter identification from imbalance response measurements

Table 1. Summary of test rotor geometry and inertia properties for imbalance response measurements

Units	*ISO*		*English*	
Rotor mass	11.8 kg		26.0 lb	
Rotor total transverse moment of inertia (I_T)	0.234 kg-m^2		800 lb-in^2	
Rotor total polar inertia (I_P)	0.030 kg-m^2		102 lb-in^2	
	mm		in	
Shaft diameter	25.4		1.00	
Shaft diameter at bearing locations	25.4		1.00	
Total length	640.0		25.20	
Bearing span	532.0		20.94	
Rotor cg location from left end	342.0		13.46	
Distances from cg to bearing locations (l_1,l_2)	263	269	10.4	10.6
Distances from cg to planes of unbalance excitation (d_1,d_2)	137	143	5.39	5.63
Radii of unbalance locations (r_1,r_2)	70.0	70.0	2.76	2.76
Distances from cg to location of proximity probes (s_1,s_2)	302	308	11.9	12.1

The rotor steel disks have a diameter equal to 165 mm (6.50 in). Each disk has an axial length of 31.9 mm (1.26 in) and weighs 3.86 kg (8.5 lb). There are 24 equally

spaced threaded holes in each disk for attachment of imbalance weights at a radius of 69.9 mm (2.75 in). The disks are attached to the shaft by means of clamping through-bolts and semi-circular lateral plates. The shaft (press-fitted) annular inserts provide support for the removable disks and locate them axially.

The bearing housings are split in the horizontal plane at the bearing centerline, and have a circumferential groove for radial oil delivery to the bearings. Split lateral covers made of aluminum provide an enclosure to avoid spills and incorporate grooves for custom stopper seals. The lubricant enters the bearings radially through slots in the partition, passes through the film lands; then falls to the bottom of the bearing housings to finally return to the main tank by gravity through the return ducts.

The rotor supports are identical, namely two-lobe, lightly preloaded, fluid film cylindrical bearings, as shown in Figure 4. Table 2 sums the bearing dimensions and operating clearance, and the lubricant material properties. The bearing back material is bronze and the liner material facing the shaft is soft babbitt metal. The free end bearing features a pair of thrust collars integral to the radial bearing. Examination of the bearings' babitted surfaces shows uneven wear that occurred in prior experiments when the bearings operated with pressurized air as the working fluid. Wear makes it difficult to precisely determine the original preload of the bearing lobes. Thus, a small nominal value of 0.05 (dimensionless) preload is used in the predictions of the bearing (linearized) force coefficients.

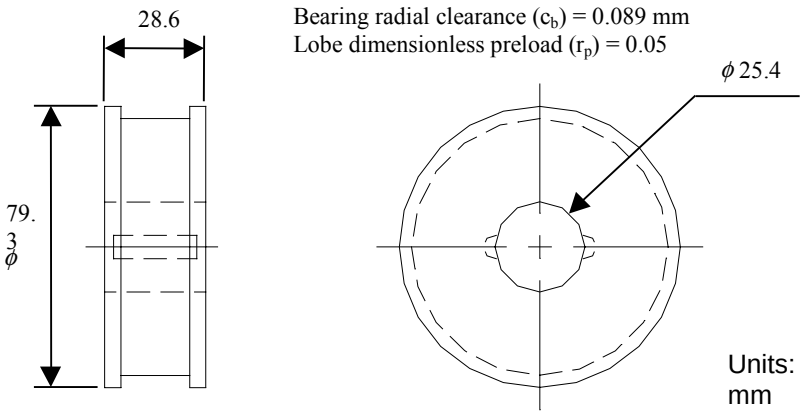

Figure 4. Two-lobe fluid film hydrodynamic bearings supporting test rotor

The lubrication system consists of a 25-lt (6.6 gal) oil tank, a submerged gear pump, pressure control valves and ducts. The oil tank is built integral with the test rig and is located at its lowest level. The gear pump delivers the lubricant (ISO VG 10 turbine oil) to the bearing housings at a supply pressure of 60 kPa (10 psig). Rigid pipelines conduct the lubricant to the bearing pedestals and a pressure gauge indicates the main inlet pressure. Lubricant temperature in the tank is measured with a handheld thermometer and recorded at the beginning and at the end of each test.

Table 2. Two-lobe bearings main dimensions and operating conditions

Bearing nominal diameter (D)	25.4 mm	1.000 in
Bearing axial length (L_b)	28.6 mm	1.126 in
Bearing radial clearance (c_b)	0.089 mm	3.5 mils
Estimated pad preload (r_p)	0.05 (dimensionless)	
Average inlet lubricant viscosity (μ)	15.76 cP	at 24.4° C (76° F)
Operating speed range:	0-4,000 rpm	
Static load		
Drive end bearing	57.9 N	13.0 lb (11.55 psi - specific load)
Free end bearing	57.9 N	13.0 lb (11.55 psi - specific load)

Measurements of the test rotor displacements are taken with two pairs of eddy current sensors located very close to the bearing centerlines. The bearing housings have threaded holes for installation of the sensors in two orthogonal directions, and located at 45° away from the vertical line, as shown in Figure 5. An additional eddy-current sensor aligned with the vertical direction and facing the rotor shaft (downwards) provides a reference signal for measurement of the phase angle and rotor speed.

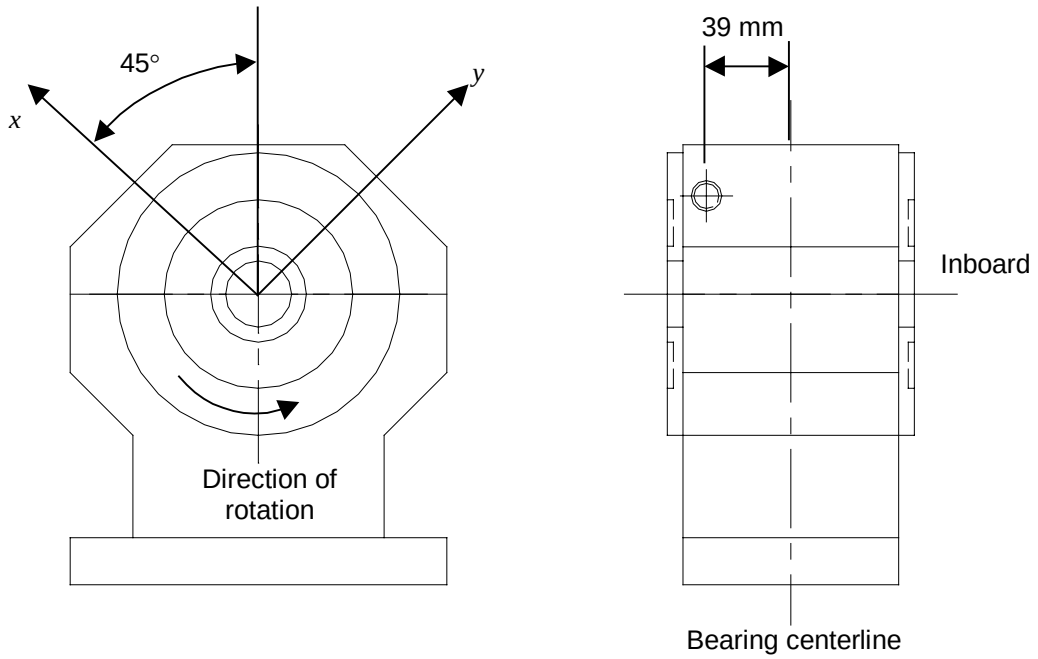

Figure 5 Bearing housing and disposition of eddy-current sensors for measurement of rotor response.

Vibration signals from the eddy current sensors connect directly into a commercial data acquisition system for industrial machinery monitoring and diagnostic (ADRE® DAQ system). A PC hosts the acquisition system and runs the signal processing and analysis software. A two-channel dynamic signal analyzer displays the frequency content of the selected signals, and analog oscilloscopes display the unfiltered rotor orbits in real time.

Test procedure for imbalance response measurements

The first procedure prior to conduct imbalance response measurements is rotor balancing. Rotor balancing is important because it provides a baseline for measurement of rotor response to calibrated imbalance masses. This is particularly important for sensitive systems because large orbital motions of the rotor at the bearings might compromise the estimation of linearized force coefficients. For the test rotors presented above, a standard influence coefficient method for two-plane balancing substantially reduces the original rotor synchronous response to satisfactory small levels of vibration.

Imbalance response tests consist of taking the rotor to a top speed and then coasting it down by shutting off the power to the drive DC motor. Measurements of rotor response are taken while the rotor coasts downs freely at a slow deceleration rate. The measured synchronous vibration vector (amplitude and phase, $\mathbf{V}_m$) at each speed is the sum of the remnant imbalance vector ($\mathbf{V}_r$), the dynamic rotor response to the calibrated imbalance ($\mathbf{V}$) and the shaft runout vector (also called slow-roll vector, $\mathbf{V}_s$). Thus, $\mathbf{V} = \mathbf{V}_m - \mathbf{V}_r - \mathbf{V}_s$ at each rotor speed (Ω)

Shaft runout is represented as a constant vector ($\mathbf{V}_s$) that acts in all tests and for the entire speed range. If the remnant imbalance vector is not slow-roll compensated from shaft runout, (this is, if $\overline{\mathbf{V}}_r = \mathbf{V}_r + \mathbf{V}_s$) then the true dynamic response to calibrated imbalance is simply $\mathbf{V} = \mathbf{V}_m - \overline{\mathbf{V}}_r$. This last relationship does not require a priori knowledge of the slow roll vector, and is the form used in the compensated responses implemented for the identification of synchronous bearing support force coefficients.

Rotor model and predicted bearing force coefficients

Figure 6 depicts the test rotor modeled as a collection of nine finite elements. The bearing support locations and planes of imbalance are noted. Note that the solid thin disks are modeled as integral shaft elements, not as added local inertias. The calculated fundamental rotor free-free mode natural frequency equals 200.5 Hz, agreeing well with a measured magnitude of 198 Hz from rap tests on the rotor. The Figure displays the static sag line due to the rotor weight and demonstrates the shaft flexibility. De Santiago [3] reports an experimental pin-pin first natural frequency equal to 76.3 Hz, while the predicted value is 78.5 Hz.

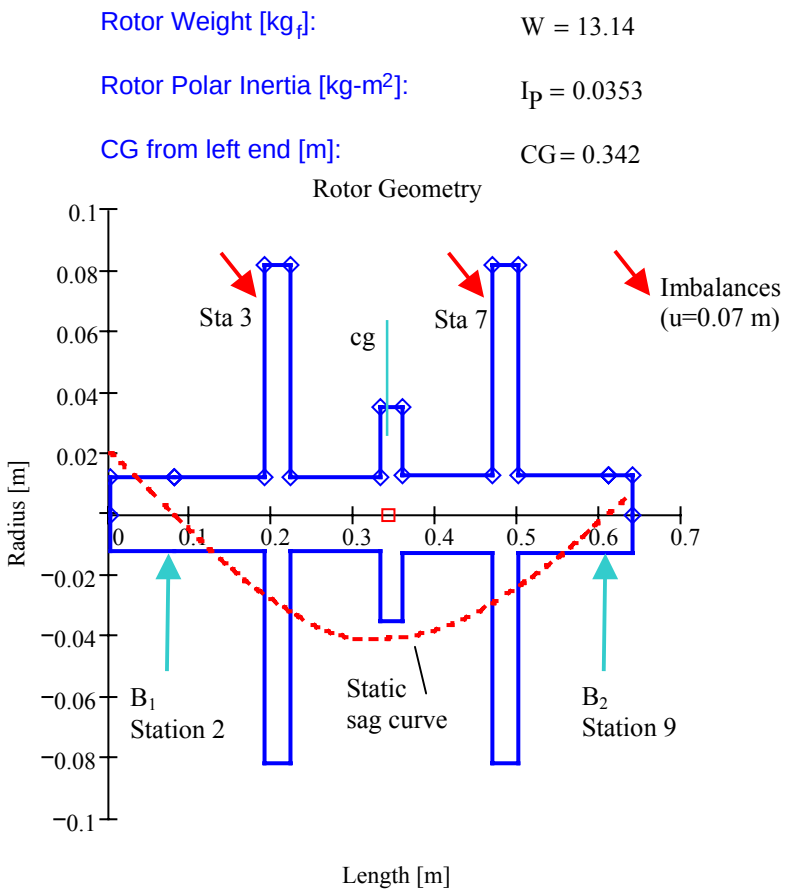

Figure 6 Rotor geometry and static deflection due to weight. Bearing locations and imbalance planes noted

The two lobe bearings are identical in geometry and share approximately the same static load. Thus, the bearing force coefficients are similar. Table 3 shows the predicted stiffness and damping force coefficients over a range of rotor speeds. XLTRC^2 XLTFPBRG program, based on the analysis given in [15], is used to obtain the bearing parameters.

Note that the predicted direct stiffness coefficients in directions (*x*) and (*y*) are different. The magnitude of the stiffness in the vertical (*y*) direction is about twice the magnitude of the stiffness in the (*x*) direction. Increased stiffness of the fluid film in the direction of the lobe pad is typical of preloaded bearings and usually aims to increase the threshold speed of instability. Cross-coupled stiffness coefficients are of opposite sign over almost the entire speed range. Rotor speed affects greatly the damping force coefficients. Note that the magnitude of the cross-coupled damping coefficients is of the same order of magnitude as the direct damping coefficients in the (*x*) direction.

Table 3. Predicted bearing coefficients of two-lobe bearings versus rotor speed [3]

Speed	K_{xx}	K_{xy}	K_{yx}	K_{yy}	C_{xx}	C_{xy}	C_{yx}	C_{yy}
Rpm	MN/m				kN-s/m			
400	1.11	-0.47	-3.02	5.55	17.05	-31.18	-31.13	131.1
1,000	1.10	0.03	-2.44	3.27	10.22	-11.69	-11.68	44.68
1,500	1.12	0.26	-2.32	2.74	7.98	-7.31	-7.30	28.96
2,000	1.14	0.47	-2.26	2.38	6.77	-5.15	-5.14	21.47
2,500	1.17	0.64	-2.27	2.24	6.07	-3.90	-3.89	17.54
2,750	1.18	0.73	-2.28	2.17	5.81	-3.45	-3.43	16.12
3,000	1.19	0.82	-2.29	2.11	5.61	-3.06	-3.05	14.97
3,250	1.20	0.91	-2.33	2.12	5.48	-2.73	-2.72	14.27
3,500	1.21	1.00	-2.37	2.13	5.37	-2.45	-2.43	13.66
3,750	1.23	1.09	-2.41	2.14	5.28	-2.20	-2.18	13.14
4,000	1.24	1.19	-2.45	2.15	5.20	-1.98	-1.97	12.68
4,250	1.25	1.28	-2.49	2.16	5.13	-1.79	-1.78	12.28
4,500	1.26	1.37	-2.53	2.17	5.06	-1.62	-1.60	11.92
4,750	1.27	1.47	-2.58	2.19	5.00	-1.47	-1.45	11.61
5,000	1.28	1.56	-2.63	2.23	4.94	-1.30	-1.28	11.39

Bearing radial clearance: 89 microns
Dimensionless preload: 0.05

Measurements of rotor imbalance are conducted for rotor speeds from 1,500 to 3,500 rpm, below the first critical speed of the rotor. Table 4 shows the mass imbalance distributions used in the two tests. Note that these imbalances will produce linearly independent rotor responses. Positive angles on the rotor are measured opposite to its direction of rotation and from rotating reference (i.e. keyway in rotor or reflective pick-up mark).

Table 4. Imbalance distributions on test rotor for parameter identification of bearing force coefficients

	Test 1 – station 3 Drive end disk	**Test 2** – station 7 Free end disk
Imbalance	10.6 gram at 0°	10.6 gram at 0°

Drive end disk: radius r_1 = 0.070 m, distance from rotor CG d_1 = 0.139 m.
Free end disk: radius r_2 = 0.070 m, distance from rotor CG d_2 = 0.141 m.

Figure 7 shows the measured synchronous (slow roll and baseline compensated) imbalance response at the bearing locations resulting from the imbalance masses attached at the rotor disk locations. Note that the measured rotor responses are at different axial planes from the bearing planes and at different radial planes, thus a suitable coordinate transformation is required from the measurements to obtain the responses presented in the figure[1]. Note also that the largest magnitudes of rotor dynamic response correspond to more than 50% of the bearing radial clearance (0.089 mm) as the rotor approaches the critical speed. The experimental responses show different amplitudes of vibration at the

[1] This certain limitation will be removed in later developments

two bearing locations as a result of the uneven imbalance distribution. In fact, amplitudes of motion at location 1 (drive end) are larger than the amplitudes of motion at location 2 (free end) because the drive end disk carries the imbalance mass.

Validation of parameter identification method using predicted rotor responses

Before proceeding to identify the force coefficients using the test data it is pertinent to validate the predictive model advanced in an earlier section. To this end, the predicted bearing force coefficients (see Table 3) are integrated into the rotor model and imbalance responses calculated for two sets of imbalances identical to those used in the measurements. Figure 8 depicts the calculated rotor responses at the two bearing planes (B_1 and B_2) over a speed range from 400 rpm to 5,000 rpm.

The predictions correlate favorably (amplitude and phase angle) with the measured responses for the speed range to 3,500 rpm. The calculated rotor responses show the approach and passage through a bending critical speed just above 3,500 rpm. Figures 9 and 10 show the predicted rotor deflected shapes for speeds equal to 2,000 and 4,000 rpm, respectively. Note that at 4,000 rpm the rotor deflections at midspan are nearly an order of magnitude larger than at the bearing locations, thus demonstrating the rotor flexibility. Even at a speed of 2,000 rpm, the rotor does show elastic deflections, and therefore rotor flexibility needs to be accounted for in a predictive model to estimate the bearing support force coefficients. Note that the measurements could not have been conducted for speeds above the maximum noted (3,500 rpm) due to excessive vibration amplitudes, potentially harmful to the structural integrity of the test rig.

In general, the predicted rotor motions at the bearing locations are somewhat larger than the measured ones, in particular at the highest rotor speeds. Recall that the predicted force coefficients are strictly valid for small amplitude motions around the static equilibrium position, typically 10% to 20% of the bearing clearance. The measurements and predictions show large amplitude motions. However, the experimental values are smaller demonstrating that the bearing reaction forces are nonlinear in character.

Equations (14) through (18) establish the algorithm for identification of support parameters. These equations are easily programmed into the MATHCAD computational tool to estimate the support force coefficients from two predicted imbalance responses, see Figure 8. Figure 11 depicts the identified stiffness and damping force coefficients at the bearing supports (B_1 and B_2) versus rotor speed. The analytical force coefficients are also shown in each graph. Note that the estimated force coefficients using the numerical data, i.e. predicted rotor responses, are identical to the stiffness and damping coefficients given in Table 3. Thus, the results demonstrate the accuracy of the identification method advanced[2]. More importantly, however, the procedure also forwards identical force coefficients for both bearing supports, as was known from the outset.

[2] The reliability of the procedure depends on the quality of the responses used which must show sufficiently large amplitudes and accurate phase angle estimations. Incidentally, the choice of linearly independent imbalance distributions is crucial to obtain reliable support force coefficients.

Bearing force coefficients estimated from measured rotor responses

Figure 12 depicts the estimated bearing force coefficients, stiffness and damping, obtained from the measured rotor imbalance responses, see Figure 7. In the identification procedure, the supports are assumed to be identical thus providing equal force coefficients. Equation (19) in the analysis is used to estimate the bearing parameters. The simplification improves the reliability of the estimations, obscured at times since the phase angles may not have been accurately recorded.

The predicted bearing force coefficients agree reasonably well with the (experimentally derived) estimated force coefficients from the measured imbalance responses. Note that close agreement is not expected, in particular at the largest rotor speeds, since the rotor motions at the bearing locations are large, with orbit amplitudes spanning more than 50% of the available bearing clearance. The direct damping coefficients (C_{xx}, C_{yy}) decrease in magnitude as the rotor speed increases, thus anticipating the subsynchronous instability, well known for this type of rotor-bearing configuration. The cross-coupled damping coefficients are negative and $C_{xy} \sim C_{yx}$, in particular at the largest shaft speed. The test cross-coupled stiffness coefficients (K_{xy}, K_{yx}) and the direct stiffness (K_{xx}) agree best with the predictions. On the other hand, the other direct stiffness coefficient (K_{yy}) is negative for most speeds, thus showing the influence of fluid inertia, i.e. significant added mass coefficients that reduce the dynamic direct stiffness of the test bearings.

Conclusions

This report presents a method for estimation of (bearing) support force coefficients in flexible rotor-bearing systems. The research continues to advance practical and reliable methods for identification of bearing support parameters in actual turbomachinery. The current method requires of two independent tests (runs) with known mass imbalance distributions on the rotor and the measurement of the rotor motion (amplitude and phase) at locations close to the (bearing) supports. The procedure relies on the accurate model of the rotor structure (stiffness and inertia matrices). The analysis takes the general equations of rotor-bearing synchronous motion and reorders them to render the bearing transmitted forces as a function of observable quantities; i.e. measurements at support locations. Then, synchronous (bearing) support force coefficients, stiffness and damping, are identified by solving a simple set of algebraic equations.

The present analysis extends the original work in [3] to flexible rotor-bearing systems, does not add mathematical complexity nor requires of additional instrumentation than that already available in most high performance turbomachinery. The accuracy of the method is first evaluated with numerical data generated for a rotor-bearing system emulating a laboratory test rig. Imbalance response measurements conducted with a two-disk flexible rotor supported on two-lobe fluid film bearings permit to validate the identification method results. The correlation of predicted bearing (linearized) force coefficients with the identified parameters is reasonable. Consider that the measured rotor orbital motions at the bearings are of large amplitude, nearly

amounting to the whole two-lobe bearing clearances; and recall that fluid film bearing rotordynamics force coefficients are strictly valid for infinitesimally small amplitude motions about a static equilibrium position.

Presently, the identification procedure restricts its attention to a flexible rotor with two supports (bearings). No additional support elements, other bearings or seals for example, have been incorporated into the rotor-bearing system model. However, the (a-priori known) dynamic force coefficients from these elements con be easily integrated into the general rotor model and the procedure remains identical for estimation of the support force coefficients. Conversely, the aim could be to identify the force coefficients from a balance piston seal, for example. In this case, measurement of the rotor response at the seal location could be used to estimate the (third) element stiffness and damping coefficients. Note that no more than two independent imbalance tests are required, irrespective of the number of rotor supports whose impedances are to be determined.

The method advanced does have limitations; the most notable one is the need of rotor motion measurements at the middle plane of the support element. Actual rotating machinery rarely incorporates sensors at these locations. Most often, displacement sensors are positioned on a (bearing) support side. This condition is of no consequence if the length of the bearing is small compared to the rotor length. Further work is recommended to extend the method for the case when the rotor response is recorded at locations far away from the bearing supports. The extension to the present model may require of a (yet to be defined) iterative procedure. As in [3], accurate measurement of the rotor amplitudes of motion, and in particular the phase angle, are mandatory for a successful and reliable identification.

Incidentally, the method, as stated, needs minimal modifications to identify frequency dependent force coefficients. The major change, however, is the physical implementation of a mechanism to impart external loads on the rotor with enough energy and frequency content. Impact loads exerted on the bearing housings could be a feasible alternative to be researched in the near future.

References

[1] De Santiago, O., and L., San Andrés, 2003, “Field Methods for Identification of Bearing Support Parameters. Part I-Identification from Transient Rotor Dynamic Response Due to Impacts”, ASME Paper GT 2003-38583, ASME Turbo-Expo 2003 Conference, Atlanta, GA, June.

[2] De Santiago, O., and L., San Andrés, 2003, “Field Methods for Identification of Bearing Support Parameters. Part I-Identification from Rotordynamic Response due to Imbalances”, ASME Paper GT 2003-38585, ASME Turbo-Expo 2003 Conference, Atlanta, GA, June.

[3] De Santiago, O., 2002, “Identification Of Bearing Supports' Force Coefficients From Rotor Responses Due To Imbalances And Impact Loads”, Ph.D. Dissertation, Texas A&M University, August.

[4] Goodwin, M. J., 1991, "Experimental Techniques for Bearing Impedance Measurement", *Journal of Engineering for Industry*, Vol. 113, Aug., pp. 335-342.
[5] Nordmann, R. and K. Shollhorn, 1980, "Identification of Stiffness and Damping Coefficients of Journal Bearings by Means of the Impact Method", *Proceedings of the International Conference on Vibration in Rotating Machinery* (ISROMAC), IMechE, Cambridge, England, pp. 231-238.
[6] Twari, R., and N.S. Vyas, 1997, "Non-Linear Bearing Stiffness Parameter Extraction from Random response in Flexible Rotor-Bearing Systems," Journal of Sound and Vibration, vol. 203 (3), pp. 389-408.
[7] Maslen, E., C. Sortore, J. A. Vásquez, and C. Knospe, 2000, "Synchronous Response Estimation in Rotating Machinery," ASME Paper 2000-GT-0397.
[8] Maslen, E., J. A. Vásquez, and C. Sortore, 2000, "reconciliation of rotordynamic Models with Experimental Data," ASME Paper 2000-GT-0395.
[9] Lees, A.W., M.I. Friswell, M.G. Smart, and U. Press, 1998, "The Identification of Foundation Vibration Parameters from Running Machine Data," 7th Int. Symposium n Transport phenomena and Dynamics of Rotating Machinery, Honolulu, pp. 715-724.
[10] Feng, N.S., and E. Hahn, 2001, "Identification of Pedestal Parameters in Rotor Bearing Systems Using Known Unbalance," proceedings of the ASME Design Engineering Conference, Symposium on Experiments with Nonlinear dynamics Systems, Papert No. DETC 2001/VIB-215553.
[11] Feng, N.S., and E. Hahn, 2001,"Numerical Evaluation of an Identification technique for Flexibly Supported Rigid Turbomachinery Foundations," 2002, IFToMM 6th Int. Conference on Rotor Dynamics, Sydney.
[12] Childs, D., 1993, "Turbomachinery Rotordynamics," John Wiley Inter Science.
[13] Nelson, H.D., 1980, "A Finite Rotating Shaft Element Using Timoshenko Beam Theory," *Journal of Mechanical Design*, Vol. 102, pp. 793-803.
[14] Holt, C., 2003, Personal communication, March
[15] San Andrés, L., 1996, "Turbulent Flow, Flexure-Pivot Hybrid Bearing for Cryogenic Applications," *Journal of Tribology*, Vol. 118, 1, pp. 190-200.

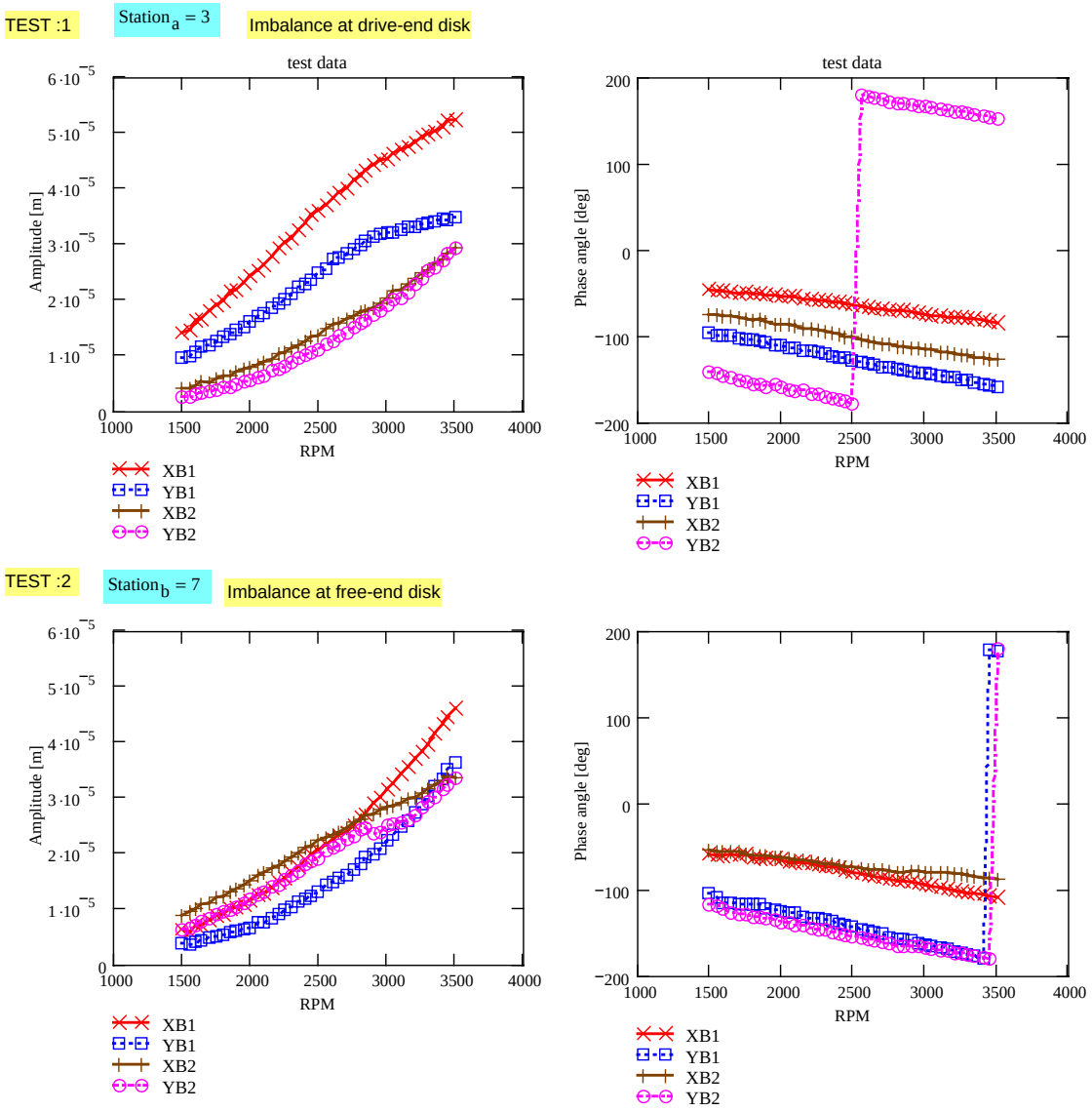

Figure 7 Measured rotor displacements (amplitude and phase) at bearing locations versus rotor speed for two imbalances (tests 1 and 2). [3]

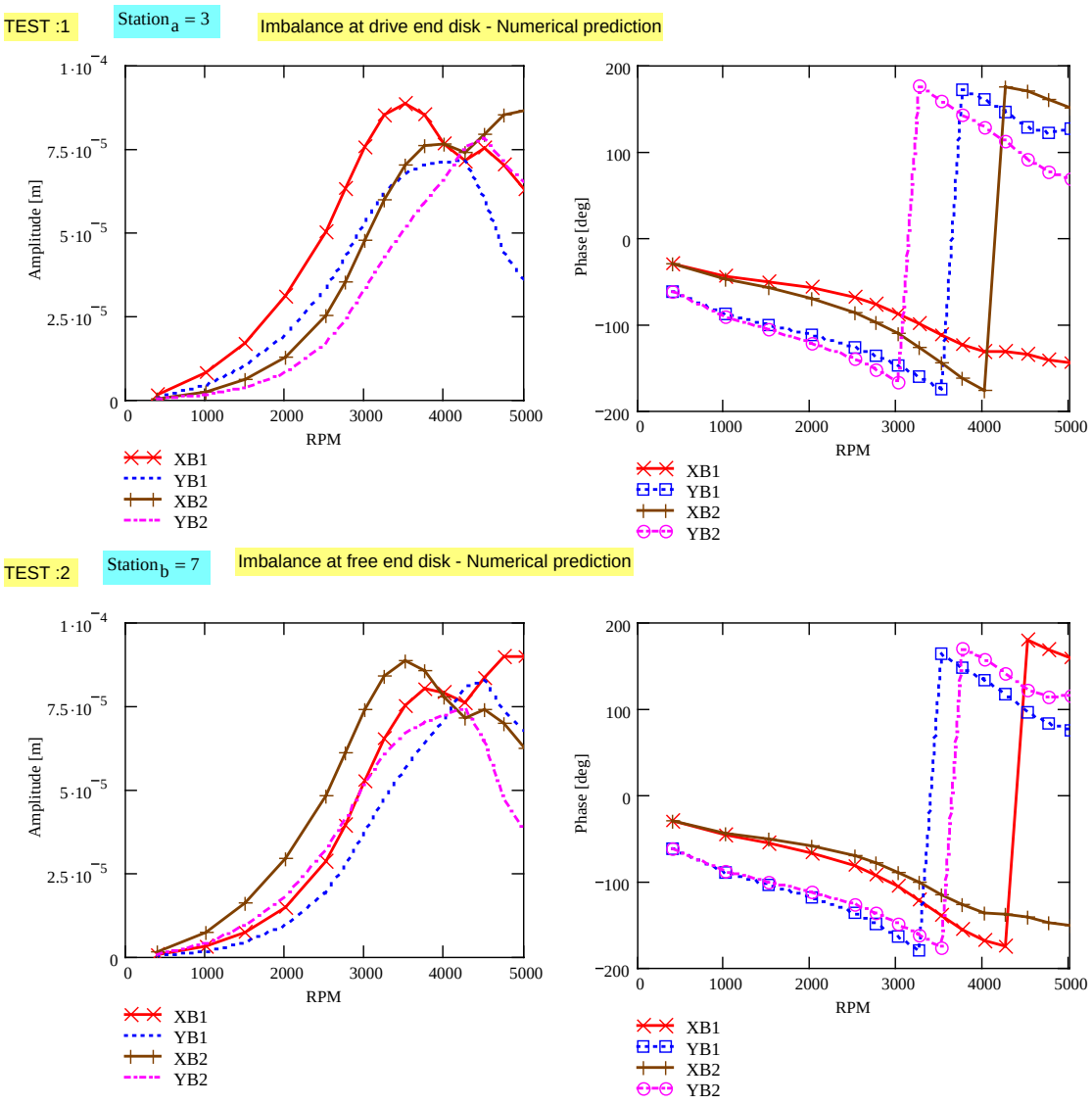

Figure 8 Predicted rotor displacements (amplitude and phase) at bearing locations versus rotor speed for two imbalances (tests 1 and 2). Numerical example.

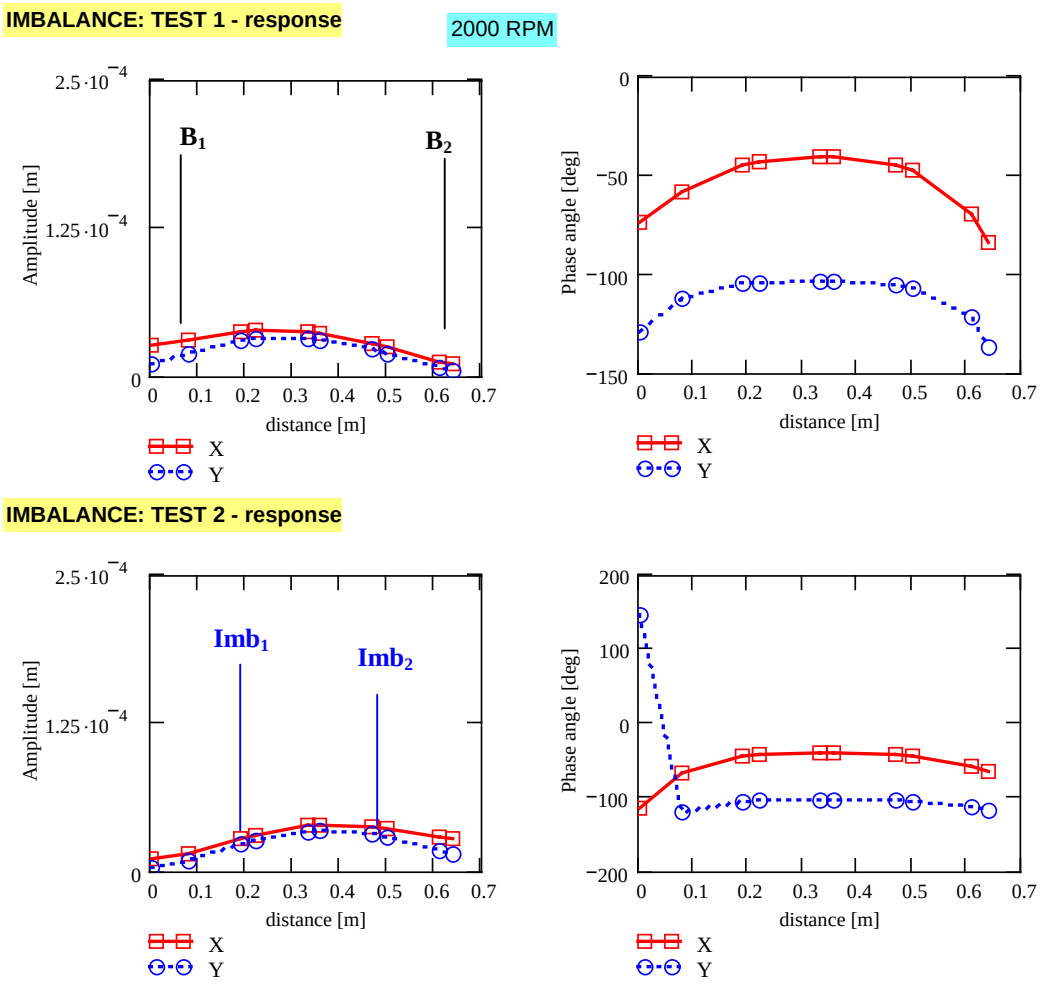

Figure 9 Predicted rotor deflection (amplitude and phase) at 2000 rpm for two imbalances (tests 1 and 2). Bearing locations noted (B_1 and B_2). Imbalances (test 1) station 3, (test 2) station 7. Numerical example

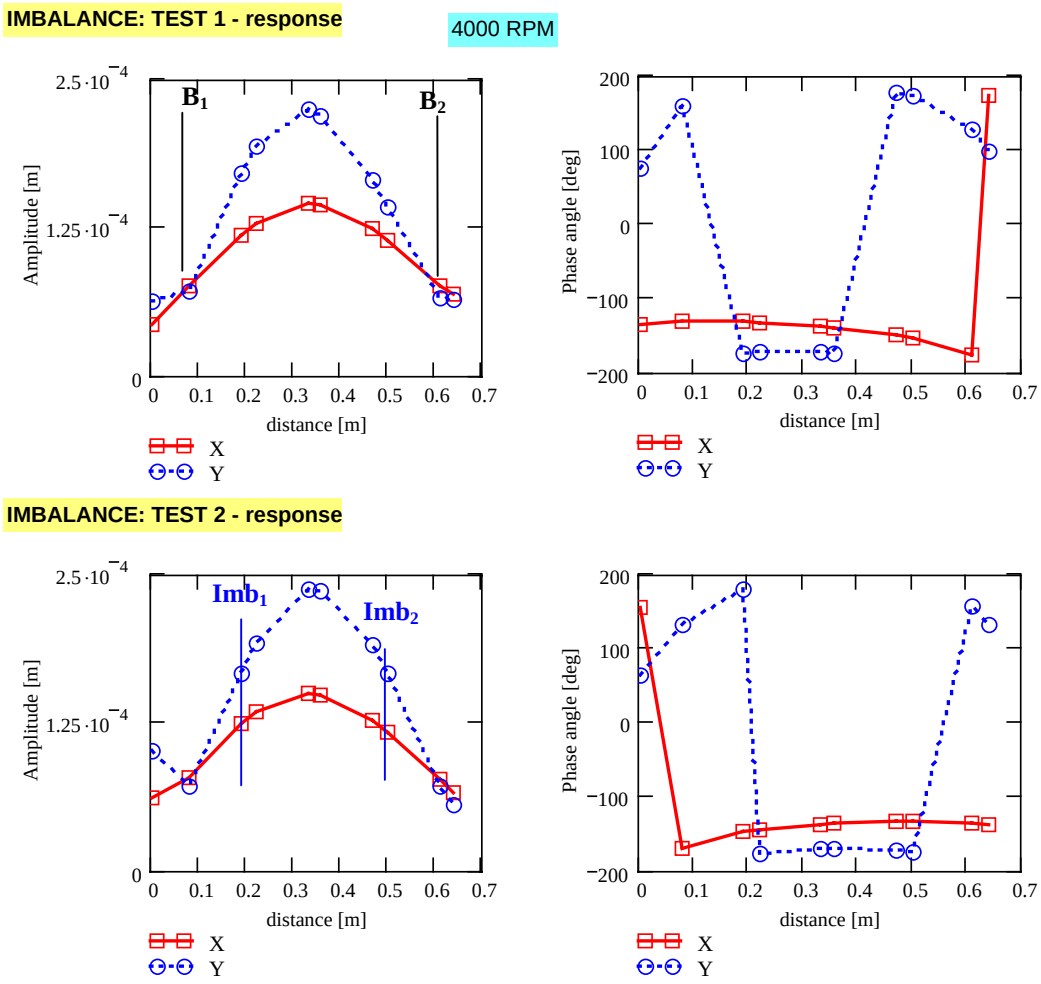

Figure 10 Predicted rotor deflection (amplitude and phase) at 4000 rpm for two imbalances (tests 1 and 2). Bearing locations noted (B_1 and B_2). Imbalances (test 1) station 3, (test 2) station 7. Numerical example

BEARINGs 1 & 2 Estimated Coefficients & Original Coefficients

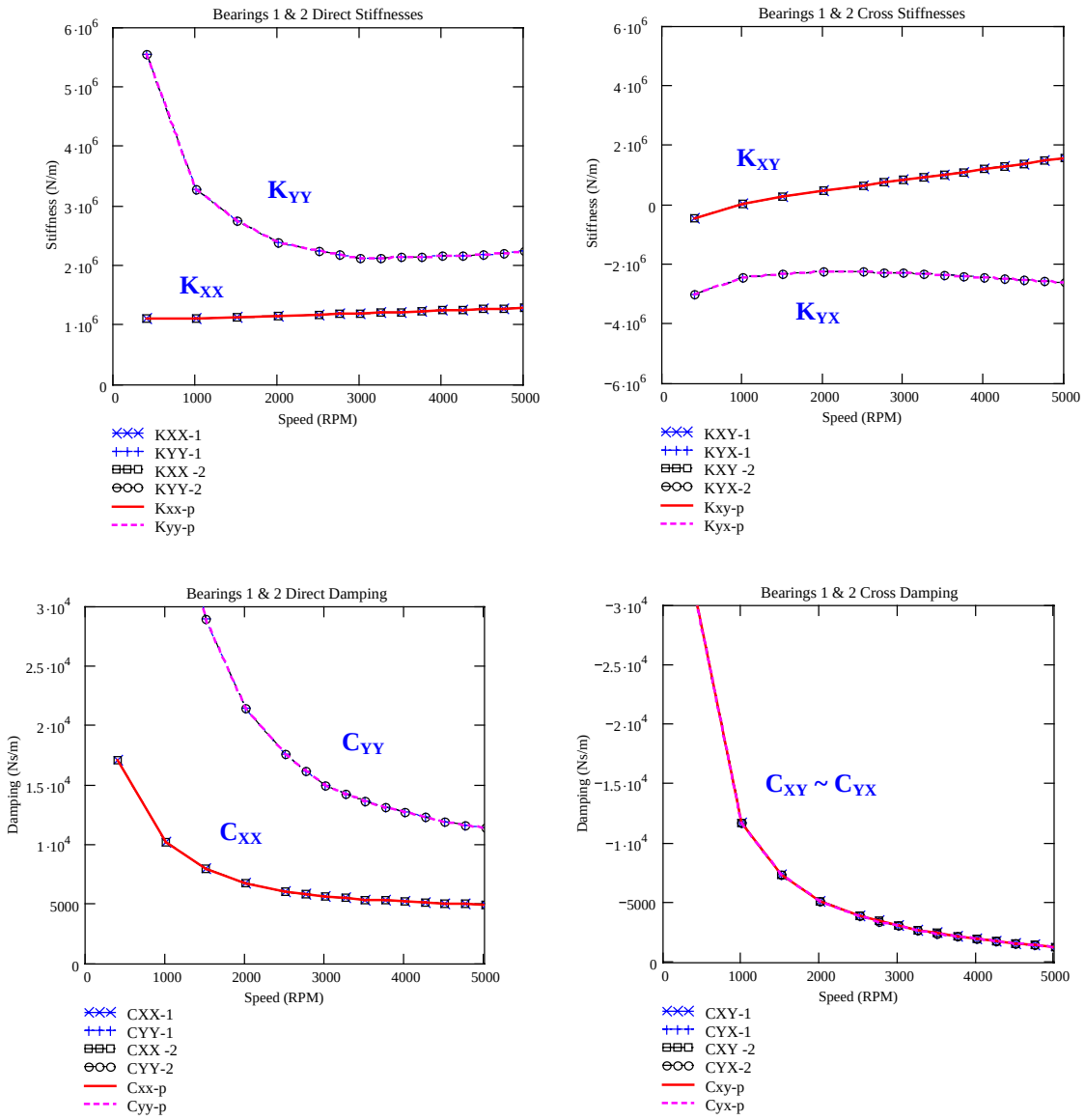

Figure 11 Estimated bearing support force coefficients versus rotor speed obtained from two predicted imbalance responses. Comparison with analytical force coefficients (Table 3). Numerical example

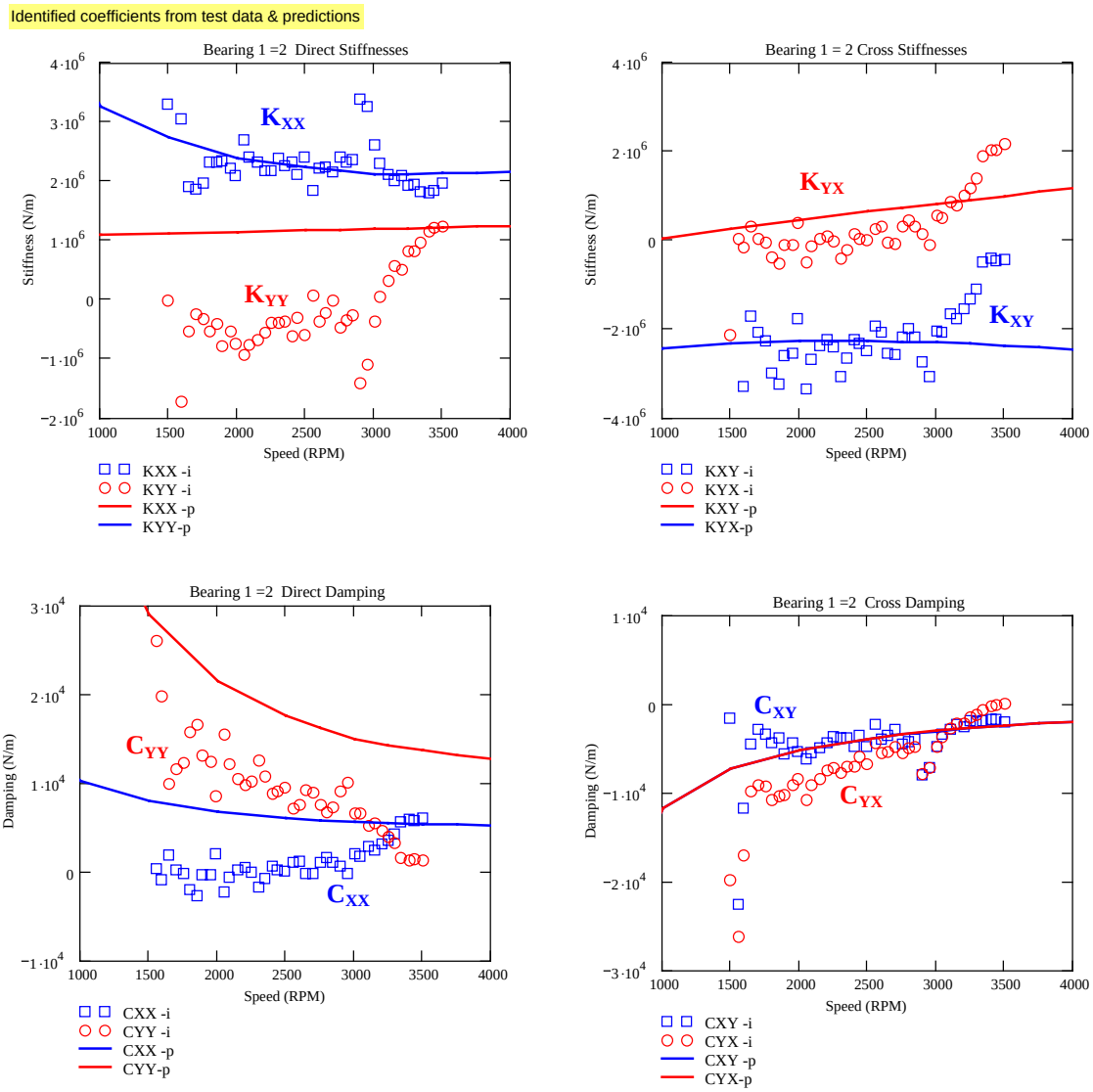

Figure 12 Estimated bearing support force coefficients versus rotor speed obtained from two measured imbalance responses. Comparison with analytical force coefficients (Table 3).
Actual test data

Appendix A.
Finite element matrices for rotor dynamics model

The element stiffness, mass, and gyroscopic matrix based on the Timoshenko beam model are defined as [13]:

$$\mathbf{K_e} = \mathbf{K_0} + \varphi \mathbf{K_1};$$
$$\mathbf{M_e} = \mathbf{M_T} + \mathbf{M_R};\ \mathbf{M_T} = \mathbf{M_0} + \varphi \mathbf{M_1} + \varphi^2 \mathbf{M_2};\ \mathbf{M_R} = \mathbf{N_0} + \varphi \mathbf{N_1} + \varphi^2 \mathbf{N_2} \qquad \text{(A.1)}$$
$$\mathbf{G_e} = \mathbf{G_0} + \varphi \mathbf{G_1} + \varphi^2 \mathbf{G_2};$$

where

Finite Element Timoshenko Beam Stiffness matrices

$$\phi(E, I, k, A, G, l) := \frac{12 \cdot E \cdot I}{k \cdot A \cdot G \cdot l^2}$$ Shear parameter function

$$K_0(E, I, l, \phi) := \frac{E \cdot I}{l^3 \cdot (1 + \phi)} \cdot \begin{pmatrix} 12 & 0 & 0 & 6 \cdot l & -12 & 0 & 0 & 6 \cdot l \\ 0 & 12 & -6 \cdot l & 0 & 0 & -12 & -6 \cdot l & 0 \\ 0 & -6 \cdot l & 4 \cdot l^2 & 0 & 0 & 6 \cdot l & 2 \cdot l^2 & 0 \\ 6 \cdot l & 0 & 0 & 4 \cdot l^2 & -6 \cdot l & 0 & 0 & 2 \cdot l^2 \\ -12 & 0 & 0 & -6 \cdot l & 12 & 0 & 0 & -6 \cdot l \\ 0 & -12 & 6 \cdot l & 0 & 0 & 12 & 6 \cdot l & 0 \\ 0 & -6 \cdot l & 2 \cdot l^2 & 0 & 0 & 6 \cdot l & 4 \cdot l^2 & 0 \\ 6 \cdot l & 0 & 0 & 2 \cdot l^2 & -6 \cdot l & 0 & 0 & 4 \cdot l^2 \end{pmatrix}$$

$$K_1(E, I, l, \phi) := \frac{E \cdot I}{l^3 \cdot (1 + \phi)} \cdot \begin{pmatrix} 0 & 0 & 0 & 0 & 0 & 0 & 0 & 0 \\ 0 & 0 & 0 & 0 & 0 & 0 & 0 & 0 \\ 0 & 0 & l^2 & 0 & 0 & 0 & -l^2 & 0 \\ 0 & 0 & 0 & l^2 & 0 & 0 & 0 & -l^2 \\ 0 & 0 & 0 & 0 & 0 & 0 & 0 & 0 \\ 0 & 0 & 0 & 0 & 0 & 0 & 0 & 0 \\ 0 & 0 & -l^2 & 0 & 0 & 0 & l^2 & 0 \\ 0 & 0 & 0 & -l^2 & 0 & 0 & 0 & l^2 \end{pmatrix}$$

Translational Mass Matrices:

$$M_0(m, l, \phi) := \frac{m \cdot l}{420 \cdot (1 + \phi)^2} \cdot \begin{pmatrix} 156 & 0 & 0 & 22 \cdot l & 54 & 0 & 0 & -13 \cdot l \\ 0 & 156 & -22 \cdot l & 0 & 0 & 54 & 13 \cdot l & 0 \\ 0 & -22 \cdot l & 4 \cdot l^2 & 0 & 0 & -12 \cdot l & -3 \cdot l^2 & 0 \\ 22 \cdot l & 0 & 0 & 4 \cdot l^2 & 13 \cdot l & 0 & 0 & -3 \cdot l^2 \\ 54 & 0 & 0 & 13 \cdot l & 156 & 0 & 0 & -22 \cdot l \\ 0 & 54 & -12 \cdot l & 0 & 0 & 156 & 22 \cdot l & 0 \\ 0 & 13 \cdot l & -3 \cdot l^2 & 0 & 0 & 22 \cdot l & 4 \cdot l^2 & 0 \\ -13 \cdot l & 0 & 0 & -3 \cdot l^2 & -22 \cdot l & 0 & 0 & 4 \cdot l^2 \end{pmatrix}$$

$$M_1(m, l, \phi) := \frac{m \cdot l}{420 \cdot (1 + \phi)^2} \cdot \begin{pmatrix} 294 & 0 & 0 & 38.5 \cdot l & 126 & 0 & 0 & -31.5 \cdot l \\ 0 & 294 & -38.5 \cdot l & 0 & 0 & 126 & 31.5 \cdot l & 0 \\ 0 & -38.5 \cdot l & 7 \cdot l^2 & 0 & 0 & -31.5 \cdot l & -7 \cdot l^2 & 0 \\ 38.5 \cdot l & 0 & 0 & 7 \cdot l^2 & 31.5 \cdot l & 0 & 0 & -7 \cdot l^2 \\ 126 & 0 & 0 & 31.5 \cdot l & 294 & 0 & 0 & -38.5 \cdot l \\ 0 & 126 & -31.5 \cdot l & 0 & 0 & 294 & 38.5 \cdot l & 0 \\ 0 & 31.5 \cdot l & -7 \cdot l^2 & 0 & 0 & 38.5 \cdot l & 7 \cdot l^2 & 0 \\ -31.5 \cdot l & 0 & 0 & -7 \cdot l^2 & -38.5 \cdot l & 0 & 0 & 7 \cdot l^2 \end{pmatrix}$$

$$M_2(m, l, \phi) := \frac{m \cdot l}{420 \cdot (1 + \phi)^2} \cdot \begin{pmatrix} 140 & 0 & 0 & 17.5 \cdot l & 70 & 0 & 0 & -17.5 \cdot l \\ 0 & 140 & -17.5 \cdot l & 0 & 0 & 70 & 17.5 \cdot l & 0 \\ 0 & -17.5 \cdot l & 3.5 \cdot l^2 & 0 & 0 & -17.5 \cdot l & -3.5 \cdot l^2 & 0 \\ 17.5 \cdot l & 0 & 0 & 3.5 \cdot l^2 & 17.5 \cdot l & 0 & 0 & -3.5 \cdot l^2 \\ 70 & 0 & 0 & 17.5 \cdot l & 140 & 0 & 0 & -17.5 \cdot l \\ 0 & 70 & -17.5 \cdot l & 0 & 0 & 140 & 17.5 \cdot l & 0 \\ 0 & 17.5 \cdot l & -3.5 \cdot l^2 & 0 & 0 & 17.5 \cdot l & 3.5 \cdot l^2 & 0 \\ -17.5 \cdot l & 0 & 0 & -3.5 \cdot l^2 & -17.5 \cdot l & 0 & 0 & 3.5 \cdot l^2 \end{pmatrix}$$

Rotary Mass Matrices:

$$N_0(m,r,l,\phi) := \frac{m\cdot r^2}{120\cdot l\cdot(1+\phi)^2}\cdot\begin{pmatrix} 36 & 0 & 0 & 3\cdot l & -36 & 0 & 0 & 3\cdot l \\ 0 & 36 & -3\cdot l & 0 & 0 & -36 & -3\cdot l & 0 \\ 0 & -3\cdot l & 4\cdot l^2 & 0 & 0 & 3\cdot l & -l^2 & 0 \\ 3\cdot l & 0 & 0 & 4\cdot l^2 & -3\cdot l & 0 & 0 & -l^2 \\ -36 & 0 & 0 & -3\cdot l & 36 & 0 & 0 & -3\cdot l \\ 0 & -36 & 3\cdot l & 0 & 0 & 36 & 3\cdot l & 0 \\ 0 & -3\cdot l & -l^2 & 0 & 0 & 3\cdot l & 4\cdot l^2 & 0 \\ 3\cdot l & 0 & 0 & -l^2 & -3\cdot l & 0 & 0 & 4\cdot l^2 \end{pmatrix}$$

$$N_1(m,r,l,\phi) := \frac{m\cdot r^2}{120\cdot l\cdot(1+\phi)^2}\cdot\begin{pmatrix} 0 & 0 & 0 & -15\cdot l & 0 & 0 & 0 & -15\cdot l \\ 0 & 0 & 15\cdot l & 0 & 0 & 0 & 15\cdot l & 0 \\ 0 & 15\cdot l & 5\cdot l^2 & 0 & 0 & -15\cdot l & -5\cdot l^2 & 0 \\ -15\cdot l & 0 & 0 & 5\cdot l^2 & 15\cdot l & 0 & 0 & -5\cdot l^2 \\ 0 & 0 & 0 & 15\cdot l & 0 & 0 & 5 & 15\cdot l \\ 0 & 0 & -15\cdot l & 0 & 0 & 0 & -15\cdot l & 0 \\ 0 & 15\cdot l & -5\cdot l^2 & 0 & 5 & -15\cdot l & 5\cdot l^2 & 0 \\ -15\cdot l & 0 & 0 & -5\cdot l^2 & 15\cdot l & 0 & 0 & 5\cdot l^2 \end{pmatrix}$$

$$N_2(m,r,l,\phi) := \frac{m\cdot r^2}{120\cdot l\cdot(1+\phi)^2}\cdot\begin{pmatrix} 0 & 0 & 0 & 0 & 0 & 0 & 0 & 0 \\ 0 & 0 & 0 & 0 & 0 & 0 & 0 & 0 \\ 0 & 0 & 10\cdot l^2 & 0 & 0 & 0 & 5\cdot l^2 & 0 \\ 0 & 0 & 0 & 10\cdot l^2 & 0 & 0 & 0 & 5\cdot l^2 \\ 0 & 0 & 0 & 0 & 0 & 0 & 0 & 0 \\ 0 & 0 & 0 & 0 & 0 & 0 & 0 & 0 \\ 0 & 0 & 5\cdot l^2 & 0 & 0 & 0 & 10\cdot l^2 & 0 \\ 0 & 0 & 0 & 5\cdot l^2 & 0 & 0 & 0 & 10\cdot l^2 \end{pmatrix}$$

Gyroscopic Matrix:

$$G_0(m,r,l) := \frac{2\cdot m\cdot r^2}{120\cdot l}\cdot\begin{pmatrix} 0 & -36 & 3\cdot l & 0 & 0 & 36 & 3\cdot l & 0 \\ 36 & 0 & 0 & 3\cdot l & -36 & 0 & 0 & 3\cdot l \\ -3\cdot l & 0 & 0 & -4\cdot l^2 & 3\cdot l & 0 & 0 & l^2 \\ 0 & -3\cdot l & 4\cdot l^2 & 0 & 0 & 3\cdot l & -l^2 & 0 \\ 0 & 36 & -3\cdot l & 0 & 0 & -36 & -3\cdot l & 0 \\ -36 & 0 & 0 & -3\cdot l & 36 & 0 & 0 & -3\cdot l \\ -3\cdot l & 0 & 0 & l^2 & 3\cdot l & 0 & 0 & -4\cdot l^2 \\ 0 & -3\cdot l & -l^2 & 0 & 0 & 3\cdot l & 4\cdot l^2 & 0 \end{pmatrix}$$

with

length	l	Elastic modulus	E
radius	r	Shear modulus	G
Area	$A = \pi r^2$	Shear factor	κ
Area moment of inertia	$I = ¼ \pi r^4$	Shear function	ϕ
Element mass	$M = A\ l\ \rho$	Material density	ρ